

In Vivo Imaging of the Brain Vesicular Monoamine Transporter

T.M. Vander Borgh, M.R. Kilbourn, R.A. Koeppe, J.N. DaSilva, J.E. Carey, D.E. Kuhl and K.A. Frey

Departments of Internal Medicine, Division of Nuclear Medicine, and Neurology and The Mental Health Research Institute, University of Michigan, Ann Arbor, Michigan

In the search for an in vivo marker of monoamine nerve terminal integrity, we investigated methoxytetrabenazine (MTBZ) as a tracer of the brain synaptic vesicular monoamine transporter (VMAT2). **Methods:** The biodistribution, metabolism and in vivo specificity of MTBZ binding were first evaluated in rodents and the human dosimetry was estimated. Subsequently, the human brain distribution of VMAT2 binding was determined in normal volunteers following administration of [^{11}C]MTBZ. Brain regional time-activity curves were obtained, and parametric transport and binding images were calculated using arterial blood sampling and a two-compartment tracer kinetic model. **Results:** Regional rat brain localization of [^3H]MTBZ 15 min postinjection was consistent with the known monoamine nerve terminal density, which demonstrated the highest activity in the striatum, lateral septum, substantia nigra pars compacta, the raphe nuclei and the locus coeruleus. At this time, chromatography revealed over 82% of brain activity, but less than 47% of plasma activity corresponded to authentic MTBZ. In vivo [^{11}C]MTBZ binding in the mouse brain was inhibited by coinjection of excess unlabeled dihydrotetrabenazine. In humans [^{11}C]MTBZ had high initial brain uptake and rapid clearance from all regions, with longest retention in areas of high VMAT2 concentration. Parametric quantification of VMAT2 density revealed the highest distribution volume in the putamen and caudate with lower values in cerebral cortex and cerebellum. **Conclusion:** Carbon-11-MTBZ is a suitable ligand for PET quantification of the vesicular monoamine transporter in the human brain.

Key Words: tetrabenazine; vesicular monoamine transporter; positron emission tomography

J Nucl Med 1995; 36:2252-2260

Monoaminergic neurons have been implicated in the pathology of diverse neurodegenerative and psychiatric diseases. Dopaminergic nigrostriatal neurons are of demonstrated importance in the initiation and control of movement (1). Pathology of these neurons is well-documented in a variety of disorders, including Parkinson's disease, multi-

ple system atrophy and related conditions (2,3). Furthermore, presynaptic dopaminergic mechanisms have been suggested as alternatives to postsynaptic hypersensitivity in schizophrenia (4). Involvement of the locus coeruleus and its cerebral cortical noradrenergic projections has been reported in postmortem studies of Parkinson's and Alzheimer's diseases (5). Serotonergic projections from the dorsal raphe are implicated in depression by the mechanisms of depressant and antidepressant drugs (6) and by studies of cerebrospinal fluid serotonin metabolites (7). A noninvasive method for accurate, quantitative determination of monoamine neuron integrity would be of great value in advancing our understanding of the pathophysiology in the above disorders. Such methodology may additionally provide a unique tool for the assessment of disease progression and its possible therapeutic modification.

The vesicular monoamine transporter (VMAT) is a candidate marker for imaging of presynaptic monoaminergic nerve terminals. Reduction of VMAT density has been demonstrated in vitro after 6-hydroxydopamine lesion of the rat striatum (8,9) and in postmortem tissues from Parkinson's patients (10). The transporter is responsible for movement of cytoplasmic monoamines into synaptic vesicles in exchange for two intravesicular protons [for review, see (11)]. The VMAT translocates all monoamines, but as 95% of monoamine nerve terminals in the normal striatum are dopaminergic, in vivo measurements of striatal binding are almost exclusively related to the dopaminergic nigrostriatal projection. Two highly related VMATs have been recently cloned and characterized: VMAT2 is limited to monoamine neurons, whereas VMAT1 is present in adrenal chromaffin cells (11). Tetrabenazine has a 10-fold greater affinity for VMAT2, whereas reserpine is equipotent for VMAT2 and VMAT1 (12). The more limited peripheral side effects of pharmacological doses of tetrabenazine in comparison to reserpine (13) may now be explained by the VMAT2 selectivity of tetrabenazine.

We have recently synthesized [^{11}C]tetrabenazine, demonstrated specific in vivo binding in the mouse brain (14,15), imaged the reduction of monoamine nerve terminals after MPTP-induced lesions of monkey striatum (16) and depicted normal human brain VMAT2 (17). Carbon-11-tetrabenazine, however, is rapidly and extensively me-

Received Nov. 21, 1994; revision accepted Mar. 14, 1995.

For correspondence or reprints contact: K.A. Frey, MD, PhD, University of Michigan Medical Center, B1G 412/0028 AGH, 1500 E. Medical Center Dr., Ann Arbor, MI 48109-0028.

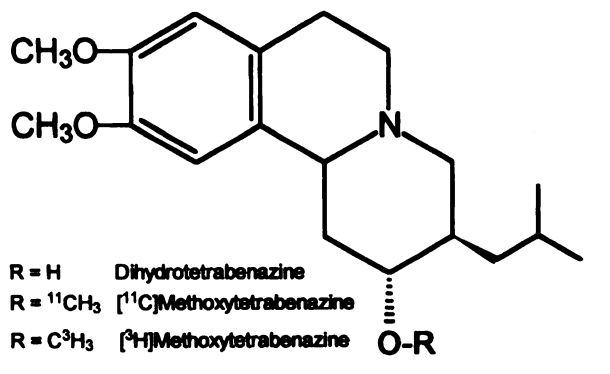


FIGURE 1. Structures of dihydrotetrabenazine, [${}^{11}\text{C}$]methoxytetrabenazine and [${}^3\text{H}$]methoxytetrabenazine.

tabolized in vivo to [${}^{11}\text{C}$]dihydrotetrabenazine. This metabolite rapidly enters the brain (18,19) and thus complicates kinetic PET modeling and quantification. Methylation of dihydrotetrabenazine, resulting in MTBZ, should circumvent the production of lipophilic labeled metabolites that interfere with analytic measurements of VMAT2 binding in vivo (Fig. 1).

The present studies evaluate MTBZ as an in vivo marker of the VMAT2 binding sites by determining its biodistribution, metabolism and specificity in rodents, followed by in vivo quantification of the VMAT2 density in normal human brain.

MATERIALS AND METHODS

Tracer Preparation

High specific activity α -[O-methyl- ${}^3\text{H}$]methoxytetrabenazine (82 Ci/mmole, 3.03 TBq/mmole) was synthesized by custom O-methylation of the normethyl precursor. Unlabeled dihydrotetrabenazine was prepared by hydrogenation of tetrabenazine purchased from Fluka Chemical Corp., Ronkonkoma, NY (16).

No-carrier-added [${}^{11}\text{C}$]MTBZ was prepared according to a method described previously by O-[${}^{11}\text{C}$]methylation of the Na-alkoxide salt of dihydrotetrabenazine (20). Radiochemical and chemical purity of [${}^{11}\text{C}$]MTBZ was >97% and specific activity determined from an analytical HPLC was routinely >35 TBq/mmole (>900 Ci/mmole) at the end of the synthesis.

MTBZ Metabolism

Three male Sprague-Dawley rats weighing 110 to 160 g were used in the evaluation of tracer metabolism and for autoradiographic imaging of in vivo brain distribution. Animals were anesthetized with diethyl ether for femoral arterial and venous catheterizations and were allowed to recover for several hours. Tritiated MTBZ [90 MBq/kg (2.5 mCi/kg)] was injected through the femoral vein as a bolus. Beginning at 14 min postinjection, arterial blood was withdrawn. At 15 min, animals were killed, the brains were rapidly removed and divided in the sagittal plane. One hemisphere was divided into forebrain and hindbrain portions for subsequent metabolite analyses using thin-layer radiochromatography (TLC). The remaining hemisphere was frozen in crushed dry ice, coated with frozen section embedding medium to prevent desiccation and stored at -70°C for subsequent cryostat sectioning and autoradiography (see below).

In chromatographic analyses, blood and tissues were homogenized in three volumes of absolute ethanol and their total activities measured by liquid scintillation spectrometry of duplicate aliquots. After centrifugation, aliquots of the supernatant were analyzed both before and after drying in an oven at 60°C and compared with activity in the original homogenate to assess recovery and the presence of volatile activity, respectively. The remaining supernatant was concentrated by vacuum centrifugation and resuspended in ethanol. The resulting concentrate as well as [${}^3\text{H}$]MTBZ standards were applied to silica TLC plates and developed with chloroform:methanol (96:4). The locations of labeled compounds were determined by contact autoradiography against radiographic film at -70°C with the use of a fluorographic enhancer (EN 3 HANCE, Dupont, Boston, MA). The identified bands were then collected for liquid scintillation spectrometry. The TLC system clearly separated MTBZ from more polar labeled metabolites. The experiments were repeated with a 200-g male Sprague-Dawley rat following administration of 370 MBq/kg (10 mCi/kg) [${}^3\text{H}$]MTBZ, in which the liver was also processed for isolation of large amounts of the radiolabeled metabolites. Together with [${}^3\text{H}$]MTBZ, they were used to develop a rapid column chromatographic procedure to isolate [${}^{11}\text{C}$]MTBZ from labeled metabolites in human plasma (see below).

The formation and identity of radiolabeled metabolites in blood was also examined after intravenous injection of 230 MBq (6.2 mCi) [${}^{11}\text{C}$]MTBZ into a monkey (*M. nemistrina*). Metabolite analysis was done using a solid-phase extraction technique (15). At 15 min after injection of [${}^{11}\text{C}$]MTBZ, a blood sample was obtained and the blood was diluted with three volumes of absolute ethanol. The mixture was centrifuged and the supernatant diluted with 9 ml 7% NaHCO_3 and applied to a Sep-Pak C18 chromatographic column (Waters Div., Millipore Corp., Milford, MA). The column was washed with 10 ml 7% NaHCO_3 , 10 ml dichloromethane and 10 ml ethanol. The dichloromethane and ethanol extracts were evaporated and the residues redissolved in ethanol, applied to silica TLC plates and developed with chloroform:methanol (96:4). Radiolabeled compounds were quantified using a scanning gamma counter.

Rodent Biodistribution of Tritiated MTBZ

Rat Brain Autoradiography. The frozen hemispheres from in vivo [${}^3\text{H}$]MTBZ injected animals (above) were processed for autoradiographic imaging of tracer distribution. Four 20- μm -thick sequential sagittal sections were collected at 200- μm intervals from each brain and were thaw-mounted on polylysine-coated microscope slides. Two of each four sections were dried on a heating plate, whereas the remaining two were dried at room temperature and then prewashed (3×3 min at 4°C) in sucrose buffer (300 mM sucrose, 50 mM Tris-HCl, 1 mM EDTA, pH 8.0 at 25°C) and briefly dipped in distilled water to remove unbound activity. Preliminary experiments demonstrated that this rinsing procedure removed the majority of nonspecific binding without loss of specific [${}^3\text{H}$]MTBZ binding (9).

Autoradiographs were generated by apposition of the adjacent washed and non-washed brain sections to tritium-sensitive x-ray film for 2 wk. Calibrated plastic radioactive standards were included with each exposure to correct for variation in exposure and development technique as described previously (21). After development, autoradiograms were analyzed by computer-assisted video densitometry. Autoradiographic film densities were converted to apparent tissue radioactivity or ligand concentrations on

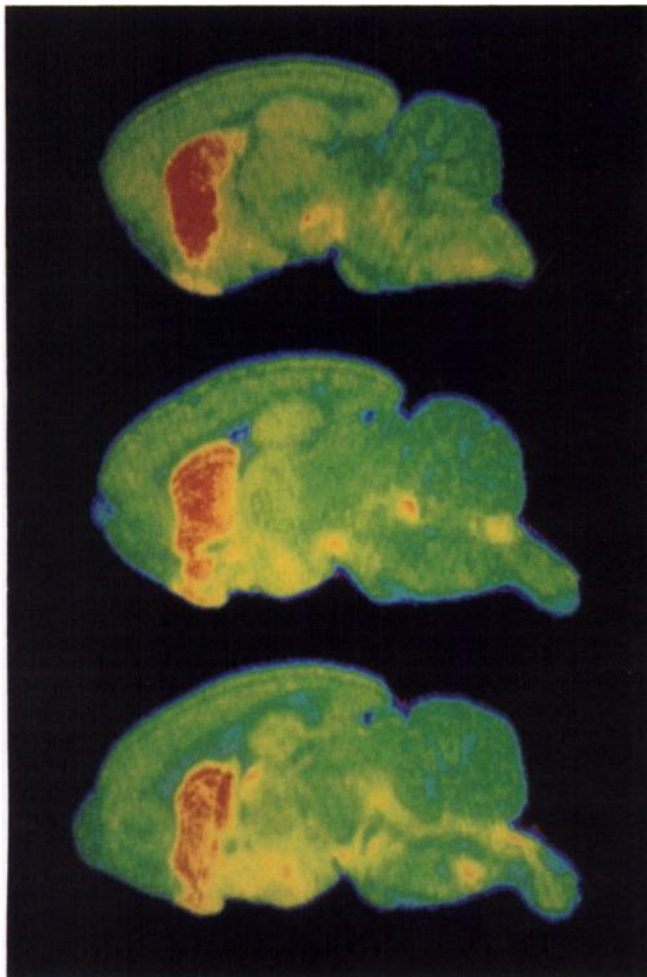


FIGURE 2. Sagittal autoradiograms of rat brain at multiple levels 15 min after intravenous injection of [^3H]MTBZ. Levels presented progress from the most lateral (top section) to medial (bottom section), corresponding approximately to levels 82, 81 and 80 of the Paxinos and Watson atlas (51). There is prominent binding in the striatum and substantia nigra pars compacta (top section) as well as the hypothalamus and locus coeruleus (middle section) and septum, ventral tegmental area and raphe nuclei (bottom section). Images are pseudocolor representations of regional tissue ligand concentration, with the highest levels represented in red and orange, intermediate concentrations in yellow and green and the lowest levels in blue and violet.

the basis of film densities overlying the radioactive standards and the specific activity of the radioligand.

Pharmacological Blocking of Carbon-11-MTBZ Uptake in Mouse Brain. The saturability of the in vivo [^{11}C]MTBZ distribution was determined in female CD-1 mice weighing 20–25 g. Two groups of four animals were injected intravenously with [^{11}C]MTBZ alone (control group) or with [^{11}C]MTBZ and an additional 10 mg/kg unlabeled dihydrotetabenazine under light diethyl ether anesthesia. Animals were allowed to awaken and were killed by decapitation 15 min postinjection. The brains were rapidly removed and dissected, followed by gamma spectroscopy and weighing with an analytic balance. Activity in each region was expressed as the decay-corrected percentage of the injected dose per g (%ID/g). Presence of regional differences in tracer distribution were assessed relative to the cerebellum using repeated measures

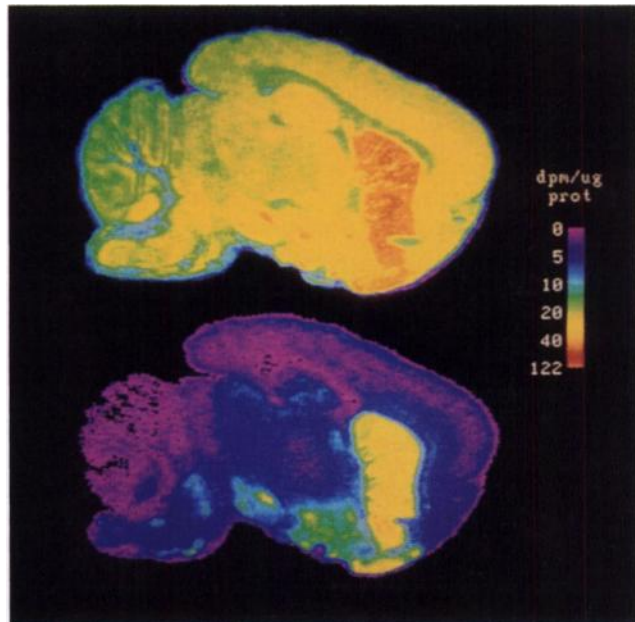


FIGURE 3. Comparison of total (top) and bound (bottom) [^3H]MTBZ activity in rat brain 15 min after intravenous tracer injection. Bound MTBZ was determined following ex vivo washing to reduce nonspecific binding and free tracer in sections immediately adjacent to those used for total activity. Images are pseudocolor representations of regional isotope concentration according to the scale on the right. Note the differential enhancement of activity in regions with the highest VMAT2 density, which correspond to the striatum, substantia nigra and hypothalamus.

ANOVA, followed by pairwise Student's t-tests, corrected for multiple comparisons by the Bonferroni method. The statistical threshold of $p < 0.05$ was considered significant.

Whole-Body Distribution in Rats. Sixteen Sprague-Dawley rats weighing 150–200 g were injected intravenously with approximately 13 MBq (360 μCi) [^{11}C]MTBZ. At 5, 15, 30 and 60 min, groups of four animals (2 males, 2 females per time point) were killed by decapitation and tissues dissected, weighed and assayed for ^{11}C activity. Radioactivity remaining in the carcass was measured in a dose calibrator. The radiation absorbed dose to humans from [^{11}C]MTBZ was estimated following the Medical Internal Radiation Dose formalism (22).

Human PET Imaging Studies

PET studies were conducted in six volunteers (3 men, 3 women aged 24–40 yr) with no significant past medical history and normal screening neurologic examination. The protocol was approved by The University Committee on the Use of Human Subjects in Research and by The University Radioactive Drug Research Committee. Written informed consent was obtained from all subjects prior to the experimental procedure.

PET scanning was performed using a Siemens ECAT-EXACT tomograph (model 921, CTI Inc., Knoxville, TN) which collects 47 simultaneous slices with intrinsic axial and transaxial resolutions of 5 mm and 6 mm FWHM, respectively. Immediately after intravenous administration of 580 ± 100 MBq (15.7 ± 2.6 mCi) [^{11}C]MTBZ (S.A.: 33 ± 11 TBq/mole; 900 ± 300 Ci/mole), images were collected according to the following dynamic sequence: 4×30 sec, 3×60 sec, 2×150 sec, 2×5 min and 4×10 min for a total of 60 min. Images were reconstructed using a Hanning filter with a cutoff frequency of 0.5 cycles/projection

element and attenuation correction was calculated by a standard ellipse fitting method, resulting in images with resolution of approximately 8 mm FWHM. Reconstructed images from all frames were reoriented to the frame acquired at 10–15 min using fiducial markers labeled with ^{11}C to correct for subject motion during the scanning session.

The peak whole-brain tracer uptake (%ID) was estimated from the product of average activity in supratentorial brain slices at 4–5 min and an assumed average brain volume of 1273 ml (23). Anatomically configured regions of interest (ROIs) were identified on the 7.5- to 10-min scan representing the caudate, putamen, thalamus and frontal and cerebellar cortices. The mean values of right and left hemisphere ROIs were used for tracer distribution analyses. The ROI boundaries were then copied to the remaining images from each dynamic sequence.

In three subjects, arterial blood samples were obtained to determine the cerebral tracer input function. At 1, 2, 3, 4, 5, 7.5, 10, 15, 20, 30, 45 and 60 min, aliquots were assayed to correct for presence of radiolabeled metabolites using a previously described procedure (24,25). Arterial blood was centrifuged and plasma, together with [^3H]MTBZ as an internal standard, was applied to conditioned Sep-Pak C18 chromatography columns. Columns were eluted with 9 ml PBS:ethanol (60:40), then with 5 ml absolute ethanol. The ^{11}C and ^3H activities in the eluted fractions were determined in a sodium iodide well counter and by liquid scintillation spectrometry, respectively. Metabolite-corrected arterial input functions were calculated from the gamma and beta assays as described previously (25). The arterial input curves and the realigned emission image sequences were analyzed according to a two-compartment tracer kinetic model, resulting in pixel-by-pixel calculation of the blood-to-tissue transport rate (K_1) and the tissue distribution volume (24).

RESULTS

MTBZ Metabolism

Fifteen minutes postinjection in the rat, $24\% \pm 2\%$ (mean \pm s.d., $n = 3$) of plasma activity and $4\% \pm 4\%$ of brain activity were attributable to labeled volatile metabolites. Recovery of homogenate activity in the ethanolic supernatant fractions was quantitative. TLC analysis of supernatants from the brain revealed that unchanged [^3H]MTBZ accounted for $82\% \pm 3\%$ of nonvolatile activity, in contrast with only $47\% \pm 8\%$ in plasma. Chromatograms revealed three groups of labeled species migrating with R_f values below authentic MTBZ. Brain chromatograms revealed minor trailing bands of activity, which corresponds predominantly to the less polar MTBZ metabolites identified in plasma. No differences in metabolite levels were observed between fore- and hindbrain samples. Chromatographic analysis of rat liver ($n = 1$ subject) revealed presence of all metabolite species identified in plasma and revealed 63% of activity corresponding to unchanged MTBZ, 12%, 8% and 8% corresponding to the three progressively more polar metabolites observed in plasma, and 9% corresponding to highly polar labeled metabolites at the chromatographic origin.

In monkey plasma, the distribution of radioactivity differed from that seen in the rat. Highly polar metabolites,

which were eluted from the chromatographic column with the aqueous wash, accounted for 38% of the total soluble radioactivity. The remaining nonpolar radiolabeled activity was unchanged [^{11}C]MTBZ, as determined by TLC analysis of the dichloromethane and ethanol fractions. In the monkey, there was no evidence for metabolites of intermediate polarity previously observed in the rat.

Isolation of the most polar labeled metabolites from rat liver (metabolites at the TLC origin and the two bands with lowest R_f values) allowed development of a rapid single-step chromatographic purification of MTBZ, which was subsequently applied in the analysis of ^{11}C containing plasma samples. The system yields better than 95% exclusion of the labeled metabolites recovered from the TLC origin with 80% retention of authentic MTBZ on the column during the initial buffer wash. There is essentially complete recovery of activity applied to the columns.

In Vivo Rat Brain MTBZ Distribution

The in vivo regional brain distribution of [^3H]MTBZ 15 min postinjection reveals highest activity in the striatum, including the caudate-putamen, nucleus accumbens and the olfactory tubercle. Other areas of intense labeling were observed in the brainstem monoaminergic nuclei, including the substantia nigra pars compacta, the ventral tegmental area, the dorsal raphe nuclei and the locus coeruleus (Fig. 2). Quantification of tracer activity revealed 75 ± 9 dpm/ μg protein in the caudate-putamen, with 31 ± 8 in the cerebral cortex and 23 ± 5 in the cerebellum (mean \pm s.d., $n = 3$). These results are consistent with the known distribution of VMAT2 density (9,26,27).

The autoradiographic results of total in vivo [^3H]MTBZ binding were compared to those following ex vivo removal of unbound tracer (Fig. 3). As expected, brief washing of the tissue following in vivo injection of [^3H]MTBZ reduced ligand activity in all regions. The decrease after washing was more pronounced in the caudate putamen than in the cortex and cerebellum (extracted activities 48 ± 8 versus 27 ± 7 and 21 ± 5 dpm/ μg protein, respectively; $p < 0.001$). The in vivo binding remaining after the washing procedure revealed the highest correlation with prior reports of VMAT2 density and was in excellent agreement with in vitro [^3H]MTBZ binding studies conducted in our laboratories (9).

Saturability of In Vivo MTBZ Accumulation

Saturability of [^{11}C]MTBZ retention in mouse brain was observed following coinjection of unlabeled dihydrotetabenazine. Blocking of VMAT2 sites by the unlabeled ligand resulted in large decreases in radioligand concentration in the striatum relative to the control (unblocked) condition. Unlabeled dihydrotetabenazine abolished regional differences in [^{11}C]MTBZ accumulation, with the exception of a minor residual distinction between the striatum and cerebellum (striatum-to-cerebellum ratio reduced from 3.0 to 1.1; Table 1).

TABLE 1
Inhibition of Carbon-11-MTBZ Binding in Mouse Brain by Unlabeled Dihydrotrabenazine*

Brain region	Control	Treated
Striatum	4.19 ± 0.50 [†]	1.50 ± 0.11 [†]
Hypothalamus	2.98 ± 0.37 [†]	1.36 ± 0.11
Hippocampus	2.04 ± 0.22 [†]	1.45 ± 0.11
Cerebral cortex	1.75 ± 0.10	1.42 ± 0.06
Thalamus	1.75 ± 0.14	1.43 ± 0.12
Cerebellum	1.42 ± 0.07	1.38 ± 0.08

*Values reflect the mean ± s.d. of measurements from four subjects in each group, expressed in units of %ID/g.

[†]p < 0.05 versus cerebellum in pairwise Student's t-test with Bonferroni correction for multiple comparisons, following identification of significant (p < 0.05) region effect in repeated measures ANOVA.

TABLE 3
Calculated Human Radiation Absorbed Dose Estimates for Carbon-11-MTBZ

Target organ	Absorbed dose	
	(mGy/MBq)	(rad/mCi)
Whole body	0.003	0.010
Red marrow	0.003	0.011
Lens of eye	0.004	0.016
Ovary	0.028	0.069
Testis	0.040	0.149
Adrenal gland	0.019	0.105
Brain	0.003	0.011
Heart	0.004	0.016
Kidney	0.017	0.063
Liver	0.014	0.052
Lung	0.003	0.012
Pancreas	0.027	0.101
Spleen	0.006	0.023
Uterus	0.003	0.010

Human Carbon-11-MTBZ Dosimetry

The rat biodistribution of [¹¹C]MTBZ (Table 2) indicated that radiotracer uptake was highest in organs involved in the presumed metabolic transformation and excretion (liver, kidneys and intestines) of the tracer. Brain uptake was maximal at 5 min (4.16% ± 0.47%) and then declined rapidly (0.72% ± 0.04% at 60 min). Essentially all of the injected dose was accounted for in the organs and carcass (99% ± 3% for all postinjection times combined). The estimated human dosimetry (Table 3) indicates gonadal tissues are dose-limiting; the most substantial absorbed dose to the less radiosensitive organs is estimated for the liver and kidney. Based on these values, an administered dose of up to 670 MBq (18 mCi) is permitted under applicable RDRC guidelines in normal volunteers.

Human PET VMAT2 Imaging

Human brain uptake and clearance of [¹¹C]MTBZ following bolus intravenous injection was rapid, with peak activity observed within 4 to 5 min postinjection (Fig. 4). At that time, whole brain uptake was approximately 9% of the administered dose, resulting in an average brain concentration of 1.8 nM and a regional brain concentration of 2.3 nM in the striatum and 1.9 nM in the cerebral cortex (Table 4). Subject 4 was excluded from this analysis due to a technical difficulty with the bolus intravenous injection, which resulted in a delay of peak brain activity. No neurologic or systemic effects of MTBZ were observed in any of the subjects.

Over the first 10 min postinjection, the brain regional

TABLE 2
Biodistribution of Carbon-11-MTBZ in the Rat*

Tissue	Time postinjection (min)			
	5	15	30	60
Adrenal	0.34 ± 0.08	0.15 ± 0.05	0.19 ± 0.04	0.13 ± 0.06
Brain	4.16 ± 0.47	1.53 ± 0.32	1.38 ± 0.08	0.72 ± 0.04
Eyes	0.09 ± 0.01	0.05 ± 0.00	0.06 ± 0.01	0.05 ± 0.01
Heart	1.08 ± 0.10	0.49 ± 0.02	0.44 ± 0.03	2.28 ± 0.00
Kidney	5.45 ± 0.64	2.45 ± 0.15	2.34 ± 0.14	2.00 ± 0.13
Large intestine	1.10 ± 0.24	0.91 ± 0.18	0.99 ± 0.08	0.85 ± 0.13
Liver	16.05 ± 2.30	17.30 ± 0.77	14.76 ± 1.23	13.94 ± 0.90
Lung	2.46 ± 0.22	1.31 ± 0.15	1.13 ± 0.22	0.59 ± 0.04
Ovary [†]	0.24 ± 0.01	0.15 ± 0.04	0.19 ± 0.14	0.14 ± 0.02
Pancreas	1.91 ± 0.31	2.19 ± 0.46	1.88 ± 0.31	1.09 ± 0.23
Small intestine	4.75 ± 1.69	5.66 ± 1.01	4.88 ± 1.35	6.23 ± 1.16
Spleen	0.80 ± 0.14	0.62 ± 0.10	0.53 ± 0.04	0.42 ± 0.09
Stomach	0.98 ± 0.13	1.88 ± 0.54	1.58 ± 0.52	1.25 ± 0.47
Testis [†]	1.02 ± 0.08	1.42 ± 0.01	1.42 ± 0.05	1.15 ± 0.04
Remainder of body	61.00 ± 0.04	66.00 ± 0.02	67.00 ± 0.03	64.00 ± 0.04

*Values reflect the mean ± s.d. of observations from four subjects per group, expressed as %ID/organ, except where otherwise noted.

[†]n = 2 subjects per group.

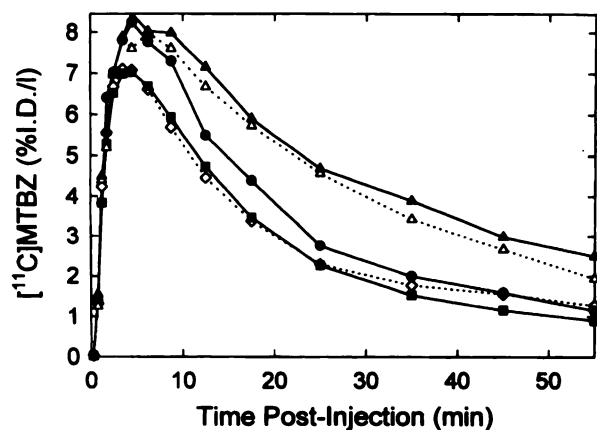


FIGURE 4. Time-activity curves, expressed as %ID/liter, from the caudate (Δ), putamen (\blacktriangle), thalamus (\bullet), frontal cortex and cerebellum (\diamond) over 60 min after injection of [^{11}C]MTBZ in a representative normal volunteer (Subject 6).

pattern of tracer uptake was consistent with that of cerebral perfusion. Distinction of white and gray matter structures was evident at these times, with only subtle differentiation between gray matter structures possessing high (striatum) versus lower (cerebral cortex and cerebellum) VMAT2 receptor density. With further progression of time, clear distinction between tracer activities in regions of known higher binding site concentration (striatum) versus regions of lower VMAT2 density (cerebellum) evolved. The striatum-to-cerebellum ratio was maximal (2.7 ± 0.4) after 45 min postinjection.

Analysis of arterial plasma samples from human studies revealed that all the activity immediately following injection was accounted for by unchanged [^{11}C]MTBZ. After 7.5 min postinjection, radiolabeled metabolites appeared in increasing relative proportion, accounting for $66\% \pm 11\%$ of total plasma activity at 60 min postinjection (Fig. 5).

The two-compartment model prediction of the blood-to-

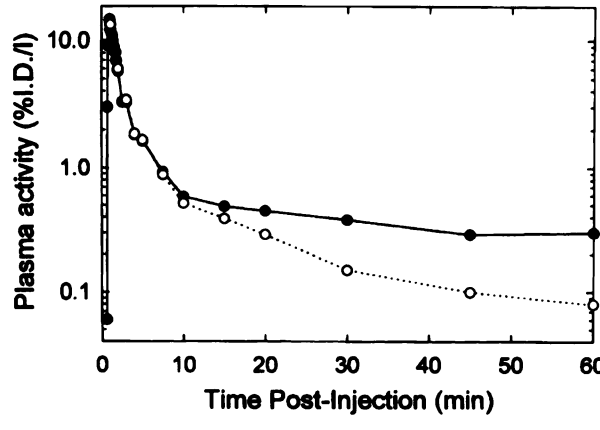


FIGURE 5. Arterial plasma time-activity curve following bolus intravenous administration of [^{11}C]MTBZ in a normal volunteer (Subject 6). Decay-corrected total plasma activity (\bullet) and activity corresponding to authentic [^{11}C]MTBZ (\circ) are shown expressed as %ID/liter. Note the early appearance and increase with time of labeled metabolites, as indicated by the difference between the curves.

brain transport rate constant (K_1) and total ligand distribution volume described the time-activity curves well. Values of K_1 averaged 0.48 ml/g/min across the gray matter regions studied, and were consistent among individuals (Table 5). The estimates of distribution volume revealed twofold differences in the binding between the striatum and cerebral cortex or cerebellum, and an intermediate level was observed in the thalamic region. Tracer kinetic parameters demonstrate better precision than the activity measures derived from summed images between 30 to 60 min postinjection (Fig. 6).

DISCUSSION

The present studies demonstrate the potential of [^{11}C]MTBZ as a non-invasive probe for measuring human brain VMAT2 density *in vivo*. Brain uptake, distribution and competitive inhibition studies in rodents reveal that

TABLE 4
Whole Human Brain Uptake of Carbon-11-MTBZ

Subject no.	Age (yr) Sex	MTBZ dose		Peak brain uptake* (%ID)	Peak brain concentration*† (nM)
		Activity (MBq)	Mass (μg)		
1	40 F	670	7.9	12.8	3.0
2	24 M	580	7.8	5.8	1.4
3	39 F	600	9.0	10.4	2.8
4	37 M	600	5.0	ND	ND
5	26 F	400	4.3	8.2	1.1
6	28 M	630	4.0	6.9	0.8

*Averaged, decay-corrected tracer activity in whole brain between 4 and 5 min postinjection, assuming a normal brain volume of 1273 ml.

†Calculated from decay-corrected whole brain average tracer activity and the injected specific activity.

ND = not determined.

TABLE 5
Regional Human Brain MTBZ Activity and Parametric Estimates of VMAT2 Density

Region	K_1^* (ml/g/min)	DV^* (ml/g)	Activity from 30 to 60 min†
			(%ID/liter)
Putamen	0.48 ± 0.02	8.4 ± 0.7	3.0 ± 1.1 (4.0 ± 1.5)
Caudate	0.47 ± 0.02	8.1 ± 1.3	2.8 ± 1.3 (3.8 ± 1.5)
Thalamus	0.49 ± 0.02	5.3 ± 0.8	1.7 ± 0.8 (2.2 ± 0.9)
Cerebral cortex	0.50 ± 0.05	4.3 ± 0.3	1.5 ± 0.7 (1.9 ± 0.7)
Cerebellum	0.49 ± 0.02	4.3 ± 0.7	1.3 ± 0.6 (1.5 ± 0.5)

*Values reflect the mean \pm s.d. of tracer kinetic parameters determined from three subjects.

†Values reflect the mean \pm s.d. of activity from the three subjects represented in the kinetic analyses. Values in parentheses reflect the mean \pm s.d. of all six subjects studied.

K_1 = transport rate; DV = distribution volume.

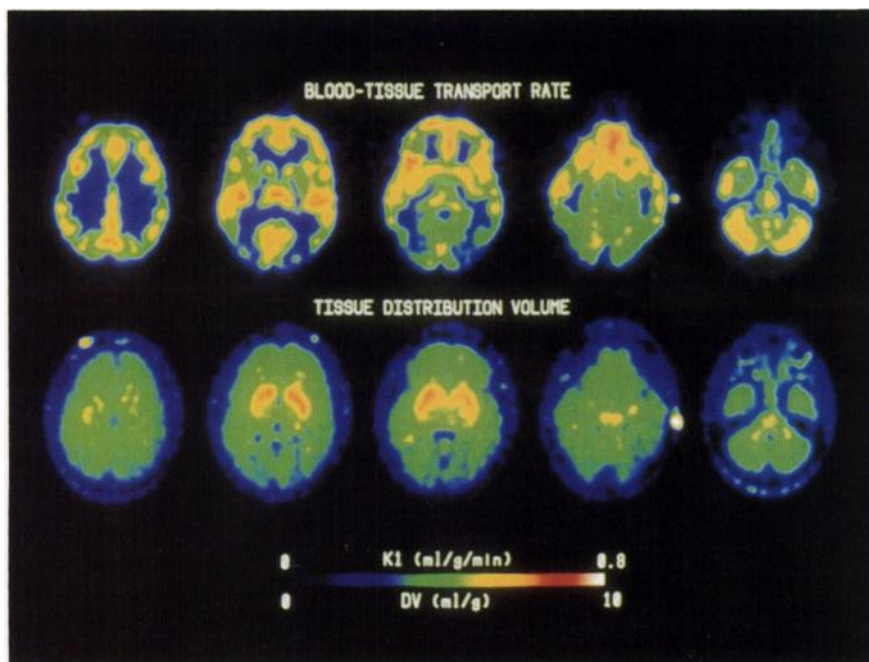


FIGURE 6. Pixel-by-pixel estimates of transport rate (K_1 , upper row, expressed in ml/g/min) and ligand distribution volume (DV, lower row, expressed in ml/g) of [^{11}C]MTBZ in normal human brain (Subject 6). Shown are five simultaneously scanned slices from the superior (left) to inferior (right) cerebral levels. Activity is displayed according to pseudocolor scales below. Note that K_1 images resemble cerebral perfusion, whereas DV images correspond to known regional densities of monoaminergic innervation. There is intense focal activity in the ventral midbrain, which corresponds to the expected location of the substantia nigra pars reticulata and ventral tegmental dopaminergic cell bodies (second image from left). The foci of activity outside the brain correspond to radioactive fiducial beads placed on the subject's scalp for dynamic image realignment purposes.

MTBZ localizes rapidly and specifically to VMAT2 binding sites. Chromatographic analyses indicate lack of interfering labeled lipophilic products in primates, which supports a straightforward interpretation of cerebral activity in PET images. Application of a two-compartment tracer kinetic model allows in vivo quantification of presynaptic monoamine binding sites in humans.

VMAT2 Ligands

Three major families of VMAT inhibitors have been identified: benzoquinolizines, reserpine and ketanserin. Among these, the benzoquinolizines, particularly dihydrotetrabenazine, have been widely used for in vitro binding studies (8,26–29). Despite a D2 dopamine receptor antagonist action at micromolar concentrations (30), benzoquinolizine binding has been shown to be a specific marker of monoamine synaptic vesicles. In contrast, ketanserin recognizes a population of 5-HT₂ receptors (8). Reserpine binding to the VMAT requires intact vesicular energy charge and pH gradient for avid binding, which is essentially irreversible. Benzoquinolizines interact with VMAT sites in a passive, readily reversible manner (28). Our selection of tetrabenazine derivatives for in vivo imaging of VMAT2 is thus based on the uncomplicated, rapid, high-affinity, reversible binding properties of these ligands.

Due to the established safety of pharmacological doses of tetrabenazine in humans, we first synthesized [^{11}C]tetrabenazine and demonstrated its ability to image in vivo intact human and MPTP-lesioned monkey striatal dopamine nerve terminals (16,17). Carbon-11-tetrabenazine, however, was found to be suboptimal for quantitative applications due to the rapid formation of an active, labeled metabolite, [^{11}C]dihydrotetrabenazine. Entry of this metabolite into the brain contributes to emission images, thus complicating pharmacokinetic analysis of radiotracer bind-

ing (15). Our present selection of [^{11}C]MTBZ is based on the reported human metabolism of tetrabenazine (18,19), which predicts that centrally active, labeled metabolites should not be produced. In contrast to the human metabolic predictions and our current nonhuman primate data, we observed presence of labeled metabolites in the rat brain following administration of [^3H]MTBZ. Metabolites accounted for less than 20% of nonvolatile activity and did not demonstrate a regionally selective distribution, which suggests a lack of VMAT2 binding activity.

MTBZ Binding to VMAT2 In Vivo

Evidence that MTBZ binds saturably to VMAT2 sites was obtained from in vivo blocking studies in the mouse. Coinjection of unlabeled dihydrotetrabenazine reduced overall cerebral uptake and abolished the regional pattern of MTBZ distribution. Other studies in our laboratories have indicated that tetrabenazine (14,15) and MTBZ biodistributions are not altered by drugs other than those directly binding to VMAT2, including dopamine receptor and presynaptic re-uptake site blockers. Both total and bound brain MTBZ distributions measured by autoradiography following in vivo administration correlated well with in vitro distribution of specific VMAT2 binding sites as assessed with [^3H]dihydrotetrabenazine (26,27). Large portions of the accumulated activity in these studies were removed by ex vivo washing of tissue sections, likely reflecting removal of unbound MTBZ and of a minor component attributable to its labeled rodent metabolites. The apparent level of nonsaturable binding in these studies is comparable to that seen in in vitro assays prior to the postincubation washing procedure. Higher levels of extracted activity were encountered in the striatum compared to the cerebral cortex or cerebellum in our ex vivo studies. This is predicted by rapid and reversible in vivo kinetics of MTBZ binding,

which predicts higher free ligand levels in close proximity to VMAT2 sites. This result emphasizes that activity measured in regions with low or absent specific binding cannot be used to accurately estimate free ligand levels in VMAT2-rich regions and that accurate determination of VMAT2 binding from emission images requires model-based kinetic analysis.

Kinetics and Modeling of MTBZ in Human Brain

Cerebral uptake, distribution and clearance of MTBZ occur rapidly in both the rodent and human brain following systemic administration. Maximal uptake is observed in human brain within 5 min postinjection and clearance half-times in the range of 16–28 min are observed across a variety of brain regions. The use of rapidly equilibrating tracers is particularly advantageous for estimation of tissue distribution volumes as an index of ligand binding, since the simplified two-compartment model used here is applicable in this setting. MTBZ is particularly well suited for ^{11}C -labeling in clinical applications; the biological and physical half-lives of ^{11}C MTBZ are comparable and permit accurate determination of both uptake and loss of tracer from all brain ROIs. Thus, a large fraction of the area under the regional tissue time-activity curves is measured within a 60-min scanning session. Consideration of the integral physiologic definition of the distribution volume (the ratio of the area under the tissue to that of the plasma tracer time-activity curves) (31) indicates that errors associated with the extrapolation of late tissue curves are likely minimal for MTBZ.

The modeling assumptions underlying the parametric binding estimates in the present work include the assumption of negligible tracer occupancy by labeled MTBZ. On the basis of prior VMAT2 B_{max} estimates obtained from ^3H dihydrotetrabenazine binding in postmortem human striatum and cortex (29), a total brain concentration of 2 nM ^{11}C MTBZ would correspond to occupation of less than 2.5% of VMAT2 in the striatum and less than 20% in the cerebral cortex. This conservative calculation assumes that all activity present is bound to the transporter, which, as demonstrated in the ex vivo rat brain washing study, is unlikely. Since PET measurements determine only the number of available VMAT2 binding sites, the possible effect of competitive occupation by an endogenous neurotransmitter must be considered. Estimates obtained in in vitro VMAT2 binding assays indicate low affinity (millimolar range) (32) binding of dopamine, thus, at expected physiologic dopamine concentrations, such competition is considered unlikely. Preliminary evidence supporting this assertion indicates lack of effect of monoamine oxidase inhibition or of L-DOPA treatment on the in vivo uptake of benzoquinolizines in the rat striatum (unpublished observations).

MTBZ binds not only to VMAT2 in dopamine nerve terminals but also to that in noradrenaline, serotonin and histamine neurons. As a result, the pattern of cerebral uptake and retention reflects binding within multiple monoaminergic systems. In the striatum, over 95% of specific binding is attributable to nigrostriatal dopaminergic terminals on the basis of lesion studies (9). The presence,

however, of noradrenergic and serotonergic projections to the cerebral cortex, hippocampus, thalamus and hypothalamus, and cerebellum preclude simple comparison of regional binding with a reference region possessing only non-specific and free tracer. Thus, quantification of MTBZ binding requires parametric estimation of brain binding relative to arterial plasma tracer activity. Due to peripheral metabolism of ^{11}C MTBZ, such binding estimates are critically dependent on correction of arterial plasma tracer activity for the presence of labeled metabolites, as accomplished here with rapid column chromatography.

Comparison to Alternative Monoaminergic Imaging Tracers

Other presynaptic imaging techniques that include ^{18}F fluoroDOPA, ^{11}C nomifensine and ^{11}C WIN 35,428 have been used to assess dopaminergic nerve terminal integrity in neurodegenerative diseases (33,34). Fluorine-18-fluoroDOPA was first used to image successively presynaptic monoaminergic nerve terminals in the human striatum (35). Its quantification, however, is complicated by the presence of labeled metabolites that contribute to the radioactivity measured by PET (36). Methods to correct for brain metabolites have been developed on the bases of a variety of assumptions (37). The use of 4- ^{18}F -L-m-tyrosine, which does not lead to such metabolites, should simplify the method (38). Because these tracers accumulate relative to DOPA decarboxylase activity, brain uptake will reflect compensatory regulation of the enzyme (39,40) in addition to dopaminergic nerve terminal density. Measurement of the plasma membrane dopamine transporter (the presynaptic re-uptake site) provides an alternative estimate of nigrostriatal synaptic integrity. Partial depletion of the transporter in parkinsonian striatum has been reported in vitro using ^3H mazindol, ^3H cocaine, ^3H GBR-12935 and ^3H WIN 35,428 (41–44). Like DOPA decarboxylase activity, however, animal studies demonstrate regulation of the re-uptake binding site following drug administration (45,46) or changes in endogenous dopamine content (47–49). In contrast, preliminary reports suggest that VMAT2 is not readily regulated, which supports its use as an index of monoamine synaptic density (50).

CONCLUSION

Carbon-11-MTBZ localizes rapidly and specifically to the brain vesicular monoamine transporter in vivo and is metabolized in primates only to polar derivatives. Therefore, ^{11}C MTBZ is a promising PET ligand for in vivo quantification of VMAT2 density in clinical research.

ACKNOWLEDGMENTS

This work was supported by grants MH47611, NS15655 and AG08671 from the National Institute of Mental Health, National Institutes of Health and the National Institute of Aging, respectively. The authors thank Phillip Sherman for his animal work on ligand specificity and the Division of Nuclear Medicine PET Center staff for radioligand production and acquisition of PET studies.

REFERENCES

- Albin RL, Young AB, Penney JB, et al. The functional anatomy of basal ganglia disorders. *TINS* 1989;12:366–375.
- Scatton B, Javoy-Agid F, Montfort JC, Agid Y. Neurochemistry of monoaminergic neurons in Parkinson's disease. In: Usdin E, Carlsson A, Dahlström A, Engel J, eds. *Catecholamines, part C: neuropharmacology and central nervous system—therapeutic aspects*. New York: Alan R. Liss; 1984;43–52.
- Polinski RJ. Multiple system atrophy. Clinical aspects, pathophysiology and treatment. *Neurol Clin* 1984;2:487–498.
- Losonczy MF, Davidson M, Davis KL. The dopamine hypothesis of schizophrenia. In: Meltzer HY, ed. *Psychopharmacology: a second generation of progress*. New York: Raven Press; 1987:745–751.
- German DC, Manaye KF, White CL, et al. Disease-specific patterns of locus coeruleus cell loss. *Ann Neurol* 1992;32:667–676.
- Gerner RH, Bunney WE Jr. Biological hypotheses of affective disorders. In: Berger PA, Brodie KH, eds. *American handbook of psychiatry*. New York: Basic Books; 1986:265–301.
- Van Praag HM. Indolamines in depression and suicide. *Prog Brain Res* 1986;65:59–71.
- Darchen F, Masuo Y, Vial M, Rostène W, Scherman D. Quantitative autoradiography of the rat brain vesicular monoamine transporter using the binding of [³H]dihydrotetraabenazine and 7-amino-8-[¹²⁵I]iodoketanserin. *Neuroscience* 1989;33:341–349.
- Vander Borgh T, Sima AAF, Kilbourn MR, Desmond TJ, Kuhl DE, Frey KA. [³H]Methoxytetraabenazine: a high specific activity ligand for estimating monoaminergic neuronal integrity. *Neuroscience* 1995;68:955–962.
- Scherman D, Desnos C, Darchen F, Pollak P, Javoy-Agid F, Agid Y. Striatal dopamine deficiency in Parkinson's disease: role of aging. *Ann Neurol* 1989;26:551–557.
- Schuldiner S. A molecular glimpse of vesicular monoamine transporter. *J Neurochem* 1994;62:2067–2078.
- Peter D, Jimenez J, Liu Y, Kim J, Edwards RH. The chromaffin granule and synaptic vesicle amine transporters differ in substrate recognition and sensitivity to inhibitors. *J Biol Chem* 1994;269:7231–7237.
- Jankovic J, Orman J. Tetraabenazine therapy of dystonia, chorea, tics and other dyskinesias. *Neurology* 1988;38:391–394.
- DaSilva JN, Kilbourn MR. In vivo binding of [¹¹C]tetraabenazine to vesicular monoamine transporters in mouse brain. *Life Sci* 1992;51:593–600.
- DaSilva JN, Carey JE, Sherman PS, Pisani T, Kilbourn MR. Characterization of [¹¹C]tetraabenazine as an in vivo radioligand for the vesicular monoamine transporter. *Nucl Med Biol* 1994;21:151–166.
- DaSilva JN, Kilbourn MR, Domino EF. In vivo imaging of monoaminergic nerve terminals in normal and MPTP-lesioned primate brain using positron emission tomography and [¹¹C]tetraabenazine. *Synapse* 1993;14:128–131.
- Kilbourn MR, DaSilva JN, Frey KA, Koeppel RA, Kuhl DE. In vivo imaging of vesicular monoamine transporters in human brain using [¹¹C]tetraabenazine and positron emission tomography. *J Neurochem* 1993;60:2315–2318.
- Schwartz DE, Bruderer H, Rieder J, Brossi A. Metabolic studies of tetraabenazine a psychotropic drug in animals and man. *Biochem Pharmacol* 1966;15:645–655.
- Mehvar R, Jamali F, Watson MWB, Skelton D. Pharmacokinetics of tetraabenazine and its major metabolite in man and rat; bioavailability and dose-dependency studies. *Drug Metab Dispos* 1987;15:250–255.
- DaSilva JN, Kilbourn MR, Mangner TJ. Synthesis of [¹¹C]methoxy derivative of α -dihydrotetraabenazine: a radioligand for studying the vesicular monoamine transporter. *Appl Radiat Isot* 1993;44:1487–1489.
- Pan HS, Frey KA, Young AB, Penney JB. Change in [³H]muscimol binding in substantia nigra, entopeduncular nucleus, globus pallidus, and thalamus after striatal lesions as demonstrated by quantitative receptor autoradiography. *J Neurosci* 1983;3:1189–1198.
- Loevinger R, Budinger TF, Watson EE. *MIRD primer for absorbed dose calculations*, revised edition. New York: Society of Nuclear Medicine; 1991.
- Davis PJM, Wright EA. A new method for measurement cranial cavity volume and its application to the assessment of cerebral atrophy at autopsy. *Neuropathol Appl Neurobiol* 1977;3:341–358.
- Frey KA, Holthoff VA, Koeppel R, Jewett DM, Kilbourn MR, Kuhl DE. Parametric in vivo imaging of benzodiazepine receptor distribution in human brain. *Ann Neurol* 1991;30:663–672.
- Frey KA, Koeppel RA, Mulholland GK, et al. In vivo muscarinic cholinergic receptor imaging in human brain with [¹¹C]scopolamine and positron emission tomography. *J Cereb Blood Flow Metab* 1992;12:147–154.
- Scherman D. Dihydrotetraabenazine binding and monoamine uptake in mouse brain regions. *J Neurochem* 1986;47:331–339.
- Scherman D, Boschi G, Rips R, Henry JP. The regionalization of [³H]dihydrotetraabenazine binding sites in the mouse brain and its relationship to the distribution of monoamines and their metabolites. *Brain Res* 1986;370:176–181.
- Scherman D, Henry JP. Reserpine binding to bovine chromaffin granules membrane. Characterization and comparison with dihydrotetraabenazine. *Mol Pharmacol* 1984;25:113–122.
- Scherman D, Raisman R, Ploska A, Agid Y. [³H]Dihydrotetraabenazine, a new in vitro monoaminergic probe for human brain. *J Neurochem* 1988;50:1131–1136.
- Reches A, Burke RE, Kuhn M, Hassan M, Jackson VR, Fahn S. Tetraabenazine, a amine-depleting drug, also blocks dopamine receptors in rat brain. *J Pharmacol Exp Ther* 1983;225:515–521.
- Lassen NA, Perl W. *Tracer kinetic methods in medical physiology*. New York: Raven Press; 1979.
- Gonzalez AM, Walther D, Pazos A, Uhl GR. Synaptic vesicular monoamine transporter expression: distribution and pharmacologic profile. *Mol Brain Res* 1994;22:219–226.
- Leenders KL, Salmon EP, Tyrrell P, et al. The nigrostriatal dopaminergic system assessed in vivo by positron emission tomography in healthy volunteer subjects and patients with Parkinson's disease. *Arch Neurol* 1990;47:1290–1298.
- Frost JJ, Rosier AJ, Reich SG, et al. Positron emission tomographic imaging of the dopamine transporter with ¹¹C-WIN 35428 reveals marked declines in mild Parkinson's disease. *Ann Neurol* 1993;34:423–431.
- Garnett ES, Firna G, Nahmias C. Dopamine visualized in the basal ganglia of living man. *Nature* 1983;305:137–138.
- Luxen A, Guillaume M, Melega WP, Pike VW, Solin O, Wagner R. Production of 6-[¹⁸F]fluoro-L-dopa and its metabolism in vivo—a critical review. *Nucl Med Biol* 1992;19:149–158.
- Hoshi H, Kuwabara H, Leger G, Cumming P, Guttman M, Gjedde A. 6-[¹⁸F]fluoro-L-dopa metabolism in living human brain: a comparison of six analytical methods. *J Cereb Blood Flow Metab* 1993;13:57–69.
- Melega WP, Perlmutter MM, Luxen A, et al. 4-[¹⁸F]fluoro-L-m-tyrosine: an L-3,4-dihydroxyphenylalanine analog for probing presynaptic dopaminergic function with positron emission tomography. *J Neurochem* 1989;53:311–314.
- Hadjiconstantinou M, Wemlinger TA, Silvia CP, Hubble JP, Neff NH. Aromatic L-amino acid decarboxylase activity of mouse striatum is modulated via dopamine receptor. *J Neurosci* 1993;60:2175–2180.
- Zhu MY, Juorio AV, Paterson TA, Boulton AA. Regulation of aromatic L-amino acid decarboxylase by dopamine receptors in the rat brain. *J Neurochem* 1992;58:636–641.
- Chinaglia G, Alvarez FJ, Probst A, Palacios JM. Mesostriatal and mesolimbic dopamine uptake binding sites are reduced in Parkinson's disease and progressive supranuclear palsy: a quantitative autoradiographic study using [³H]mazindol. *Neuroscience* 1992;49:317–327.
- Pimoule C, Schoemaker H, Javoy-Agid F, Scatton B, Agid Y, Langer SZ. Decrease in [³H]cocaine binding to the dopamine transporter in Parkinson's disease. *Eur J Pharmacol* 1983;95:145–146.
- Janowsky A, Vocci F, Berger P, et al. [³H]GBR-12935 binding to the dopamine transporter is decreased in the caudate nucleus in Parkinson's disease. *J Neurochem* 1987;49:617–621.
- Kaufman MJ, Madras BK. Severe depletion of cocaine recognition sites associated with the dopamine transporter in Parkinson's diseased striatum. *Synapse* 1991;9:43–49.
- Scheffel U, Steinert CL, Kuhar MJ, Neumeyer JL. Effect of endogenous dopamine on ³H-WIN 35428 binding to dopamine uptake sites. *J Nucl Med* 1991;32:1096.
- Kilbourn MR, Sherman PS, Pisani T. Repeated reserpine administration reduces in vivo [¹⁸F]GBR 13119 binding to the dopamine uptake site. *Eur J Pharmacol* 1992;216:109–112.
- Ikegami H, Prasad C. Neuropeptide-dopamine interactions. V. Cyclo(His-Pro) regulation of striatal dopamine transporter complex. *Peptides* 1990;11:145–148.
- Sharpe LG, Pilote NS, Mitchell WM, De Souza EB. Withdrawal of repeated cocaine decreases autoradiographic [³H]mazindol-labeling of dopamine transporter in rat nucleus accumbens. *Eur J Pharmacol* 1991;203:141–144.
- Wilson JM, Nobrega JN, Carroll ME, et al. Heterogeneous subregional binding patterns of ³H-WIN 35,428 and ³H-GBR 12,935 are differentially regulated by chronic cocaine self-administration. *J Neurosci* 1994;14:2966–2979.
- Naudon L, Leroux-Nicollet I, Costentin J. Short-term treatments with haloperidol or bromocriptine do not alter the density of the monoamine vesicular transporter. *Neurosci Lett* 1994;173:1–4.
- Paxinos G, Watson C. *The rat brain in stereotaxic coordinates*. London: Academic Press; 1982.